25X1

25X1

25X1

FINAL REPORT

ON

AUTOMATIC FOCUSING SYSTEM

November 1965

TABLE OF CONTENTS

[redacted]

25X1

LIST OF ILLUSTRATIONS

25X1

1.0 Introduction.

This report covers work done during the period of March 11, 1965 to June 11, 1965, and later tests on the application and use of solid state sensors for an Automatic Focusing System. The chief requirement for this system was that it require no special focusing targets, but should work with any input imagery; that no mechanical scanning motions be necessary; that it be capable of developing an electronic servo signal for driving the system into focus. Furthermore, this project being of limited scope both in time and money, was directed towards demonstrating basic feasibility rather than the development of a breadboard or prototype apparatus. These objectives were fully achieved.

2.0 Summary of Work Performed.

2.1 Correlation System.

Originally, the basic concept of an Automatic Focusing was predicated on the utilization of an autocorrelation technique. It relied on the fact that maximum autocorrelation is obtained when an image is in sharp focus. It was further planned to utilize a solid state image correlator as the basic sensor. Such a correlator had previously been developed by Newtek. After several weeks of work, this approach had to be abandoned. While the concept is perfectly valid, it turned out that the configuration of the solid state correlator is such that it does not perform a strict product correlation; i.e. compute the integral,

$$\iint f(x,y)\, f(x+a,\, y+b)\, dx\, dy$$

25X1

Rather, the output of the correlator is proportional to,

$$\iint \frac{f(x,y)\,f(x+a,\,y+b)}{f(x,y)+f(x+a,\,y+b)}\,dx\,dy$$

It seemed, initially, that the denominator terms may be neglected. This, however, turned out not to be so for the autofocus application.

2.2 Non-Linear Photoconducting Sensor.

Fortunately, all was not lost when the initial scheme proved unworkable because during this initial effort it became apparent from our measurements that the photoconducting materials used in the correlator exhibited a relatively high degree of non-linearity. A second approach thus evolved which utilized this non-linear behavior.

This scheme is best illustrated with a photoconductor having a square law response to light intensity. For such a sensor the output signal is proportional to,

$$\iint [f(x,y)]^2\,dx\,dy$$

This is the same as the output of a perfect product correlator. Actually, a square law response is not essential. Any sensor which has an n-th power law where n is not unity, is usable. Best sensitivity, however, is obtained when n differs from unity by a substantial margin. In the case of cadmium sulfide photoconductors, the power law can be controlled in the sensor preparation by careful control of the dopants added to the photoconductor. Sublinear behavior can also be obtained by properly controlling the thickness of the photoconductive film, or by backing up this film with another semiconductor film having a resistivity which is intermediate between the light and dark resistivities of the photoconductor.

In the course of this effort we obtained panels which had sublinear behavior and whose power law was $n = 1/2$. These were then used in the system and a servo signal was obtained which could be utilized to drive the system into focus.

2.3 Sensor Development.

The key element in the autofocus system is the photosensor which has the requisite power law behavior. Many different sensor types may be applicable. Our work was concentrated on the use of a photoconductive sensor. This was further confined to CdS and CdSe which appear to have most promise. The first phase of sensor development concentrated on depositing thin layers of photoconductor by blading onto a substrate a mixture of photoconductive powder in a silicon rubber matrix. Panels prepared by this method proved barely sufficient to demonstrate the principle. Their main drawbacks were a lack of reproducible behavior between panels prepared under substantially identical conditions; different aging effects between panels; noisy signal outputs. The physics of these "binder" panels is not well understood and it is, therefore, difficult to predict what changes in the preparation method would improve their behavior. These "binder" panels were sufficient, however, to demonstrate the soundness of the basic principles underlying the system.

The next phase in the sensor development was directed towards obtaining more reproducible and reliable behavior. To this end it was decided to prepare panels using sintered photoconductive powder layers. Such panels were successfully made and did, indeed, prove to be quite superior to the binder panels. Final demonstration of system feasibility was accomplished, using these sintered thin film layers.

2.4 Optical Testing System.

In order to be able to test the autofocus system, a special optical test rig is required. This consists of an objective lens, beam splitter, sensor mounts and several mirrors. In the course of this project such a test bed was designed and built. It proved satisfactory for our purposes. The output signals were measured and plotted and, in some cases, displayed on an oscilloscope and photographed.

[redacted]

3.0 Detail Technical Discussion.

3.1 Autocorrelation System for Autofocus.

The basic principles involved in the autofocus systme, utilizing the autocorrelation approach, were described in [redacted] Proposal N64-22 and will not be repeated here. This approach could not be used with the solid state sensor of the "photoconductive sandwich" type. The reason for this was described in the interim progress report and briefly mentioned in the introductory section above. The following points should be noted:

1) several correlation panels were made and tested;
2) these panels, since they are not true product correlators, could not be used for the autofocus application, but they are nevertheless applicable for the automatic registration of two images;
3) if, at some future time, true product correlator panels could be prepared, they would be of use for automatic focusing.

The correlation panels which were made were of the sandwich type and were prepared by imbedding the photoconductive powder in a silicone rubber binder. A typical result obtained is shown in Figure 1. This is the correlation curve of a single bar. Correlation curves of periodic bar targets were also obtained with the experimental panels. The results were in accordance with theory.

A fair amount of theoretical work was done in order to predict the behavior of these correlator panels for different target images. This work is mostly mathematical

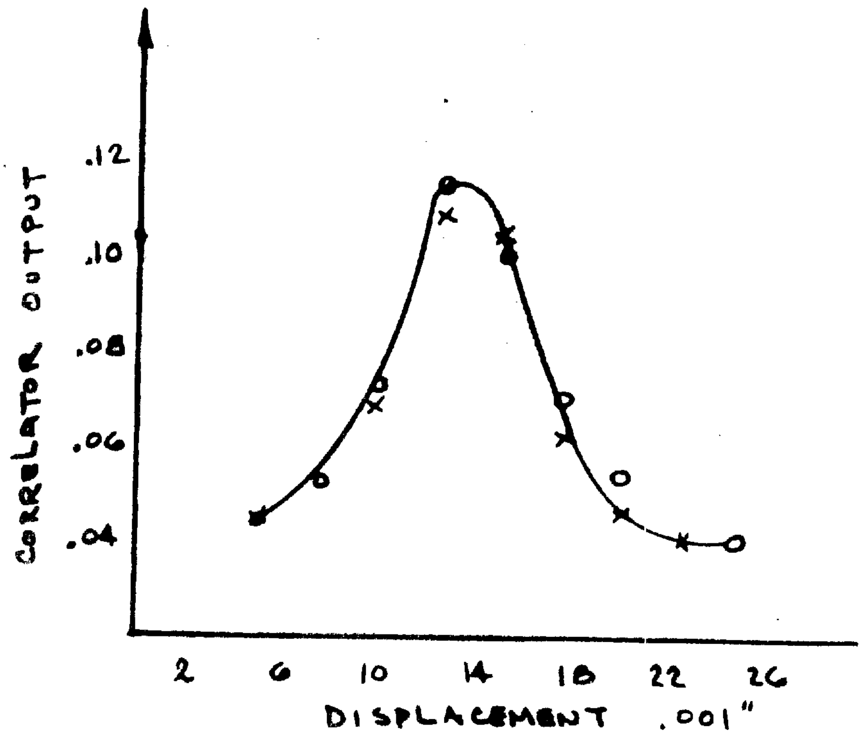

FIG 1 CORRELATION CURVE

25X1

and will be found in Appensix A. This theory is still applicable to the problem of automatic registry of images by the use of these panels. The results of this mathematical analysis are as follows:

1) The correlation curve has a maximum when the images are in register.

2) The sharpness of this correlation peak depends on the amount of detail contained in the image. With more detail, the peak will be sharper.

3) The sharpness of the peak also improves as the average contrast in the image increases.

3.2 Non-Linear Photosensors for Autofocus.

The approach which was finally adopted for implementation of the autofocus system was to utilize a non-linear photosensor. In the progress report it was stated that "it may be shown" that either a sublinear or superlinear panel may be used. We wish to presently demonstrate this fact, inasmuch as it forms the very basis of the system. To facilitate the analysis, only a point image and Gaussian spread function will be considered. The proof may, however, be extended to any image and any realizable spread function.

If a point image is defocussed by a system having a Gaussian spread function, then the resulting distribution of light intensity on the panel will be given by (one dimension is treated for ease of manipulation),

$$I = \frac{1}{\sqrt{2\pi}\,\sigma} e^{-\frac{x^2}{2\sigma^2}}$$

25X1

If the panel has an n-th power law response, then the output signal will be,

$$S = \int_{-\infty}^{\infty} I^n dx = \int \frac{1}{(2\pi)^{n/2}\sigma^n} e^{-\frac{nx^2}{2\sigma^2}} dx ,$$

$$= \frac{1}{(2\pi)^{\frac{1}{2}(n-1)}\sigma^{n-1} n^{\frac{1}{2}}} \int \frac{1}{(2\pi)^{\frac{1}{2}}\sigma_1} e^{-\frac{x}{2\sigma_1^2}} ,$$

$$= \frac{1}{(2\pi)^{\frac{1}{2}(n-1)} n^{\frac{1}{2}} \sigma^{n-1}} = \frac{\sigma^{1-n}}{(2\pi)^{\frac{1}{2}(n-1)} n^{\frac{1}{2}}} = K_n \sigma^{1-n} ,$$

where we had set,

$$K_n = \frac{1}{(2\pi)^{\frac{1}{2}(n-1)} n^{\frac{1}{2}}}$$

We now wish to study the shape of the output signal, S, as a function of the width of the spread, σ , and the power law, n . If we plot S as a function of σ with n as a parameter, it is apparent that the curves have a peak or trough at $\sigma = 0$. For a superlinear panel $(n > 1)$ the output signal will peak when for a sublinear one $(n < 1)$ the curve will be a minimum. Of course, $\sigma = 0$, corresponds to the least spread or best focus. Another way to see this is to differentiate S.

$$\frac{dS}{d\sigma} = (1-n) K_n \sigma^{-n}$$

For, σ, small the slope of the curve will be proportional to $(1-n)$. This is positive for $n < 1$ and negative for $n > 1$. A point worth noting is that the slope near $\sigma = 0$, is,

$$\frac{dS}{d\sigma} = \frac{(1-n)}{(2\pi)^{\frac{1}{2}(n-1)} n^{\frac{1}{2}} \sigma^{n}}$$

This increases very fast with n. Thus, the more superlinear the panel is, the better its sensitivity to focusing.

3.3 Photosensor Development.

3.3.1 Non-Linearity in Photoconductors.

When radiation of sufficient quantum energy is absorbed by a semiconductor or insulator, an increase of electrical conductivity results. The effect of the radiation, or light in our case, is either to increase the density of free carriers or to decrease the resistance of barriers in the material. When barriers are not present, the absorption

Sanitized Copy Approved for Release 2011/05/25 : CIA-RDP78B04747A002600020010-1

25X1

of light ionizes host-crystal atoms, producing free electrons and free holes, or it ionizes impurity atoms, producing free charge carriers of only one sign. The presence of barriers creates space charge layers which inhibit the passage of current. The action of light in this case is to decrease the barrier height. A figure of merit for a photoconductor is given by the product $T\mu$. Here, T is the lifetime of a free charge carrier, and μ is the mobility of the charge carrier. The mobility is a function of the bulk material, whereas the lifetime is dependent upon the imperfections. Usually a distinction is made between primary and secondary photocurrents. A primary photocurrent is produced directly by the ionization. The free carriers travel toward the electrodes, where they are absorbed. If there is an ohmic contact to the electrodes, current may be supplied from there to the photoconductor, in response to the primary current. These are secondary currents. The secondary current continues until the charge carrier is re-absorbed by an impurity or by a carrier of opposite sign. The presence of secondary currents gives the maximum limit to the photosensitivity.

At a given light input, the photocurrent as a function of applied voltage may be divided into three regions. At low voltage the current varies faster than linear, sometimes as the square of the voltage; at medium voltage, the relation is linear; at high voltage the photocurrent saturates. At constant voltage, the photocurrent as a function of light input may usually be divided into two regions, in each of which the photocurrent varies as some power of the light input. The low level region is generally sufficient for our purposes. In many photoconductors, the photocurrent varies linearly with light input. This is characteristic of materials in which only one free carrier is involved. In others, the current varies as the square root of the light input. This is characteristic of materials in which both free carriers are involved. In still other materials, the variation of the photocurrent with light input is some power between 0.5 and 1.0, especially 0.7 to 0.9. This is caused by traps; the variation is sensitive to the distribution of the traps. In several materials, the variation is greater than linear; powers as high as 3 have been found experimentally. This results from an increase in sensitivity with increasing light intensity, caused by a decrease in the probability of capture of a free carrier by carriers of opposite sign.

3.3.2 "Binder" Panels.

In the first attempt at demonstrating system feasibility, the photosensor used was a photoconductive layer which was prepared by dispersing CdS powder in a silicone rubber base. To get the proper consistency, a mixture of 4 grams rubber to one gram of powder was usually satisfactory. Just before spreading this onto a NESA slide, a drop of catalyst was added to the mixture. A "Doctor's blade" device was used to obtain a layer of controlled thickness. By controlling the doping of CdS, it was hoped to obtain the desired non-linearity. Doping with copper in amounts ranging from one part per million to a thousand parts per million was tried. With the high concentration of dopants super linear response was expected. The results with all the binder panels showed, however, a sublinearity of about $n = 0.5$. This was nevertheless sufficient to show that the method works in principle. It was demonstrated to the project personnel that a minimum signal output is obtained for sharpest focus.

Unfortunately, the "binder" panels had the following drawbacks:

1) Noisy signal output.
2) Drift with age and temperature.
3) Non-uniform aging rates for panels prepared in identical manner.
4) Sublinear response.
5) Non-uniformity of response at various areas on the panel.
6) Low light to dark ratios.
7) Unreliable contacts between electrodes and photoconductor.

In view of these problems, it was decided to accelerate the development of the sintered photoconductive layers for the autofocus application. Most of the problems with the binder layers were thought to be due to the fact that each powder particle was coated with a thin insulating layer of rubber. Conduction across such "blocking" barriers may be responsible for the effects that were observed.

25X1

3.3.3 Sintered Panels.

The problem of "blocking" interparticle contacts is avoided by the use of sintered photoconductive layers. These are prepared by adding a "flux" to the photoconductive powder, spreading a layer of powder onto the NESA slide, and then firing this layer for about six minutes at a temperature of 590°C. It is generally believed that the CdS is slightly soluble in the flux material at the sintering temperature. This ensured good interparticle contact. Sintered panels prepared in this manner were greatly superior to the binder panels and enabled us to obtain good autofocus performance. Still, there remain the following two problems to be solved before the sintered panels can be used effectively in an operational autofocus system.

1) Elimination of pinholes in the sintered layers or alternately to perfect a method whereby a uniform electrical contact can be applied to a layer with pinholes, but which does not short-circuit the panel.

2) Perfecting the technique for adding the flux so that the flux concentration is uniform over the area of the panel.

Despite these two outstanding difficulties, we found it possible to select some panels which were sufficiently devoid of these problems to allow their use for the tests of the autofocus system.

3.4 Testing and Evaluation.

In the course of the program, an extensive series of tests were performed on the panels in order to assess their quality. Approximately 50 panels were made and most of them were tested for their photo response, uniformity and linearity. Those which were found promising were then used in the autofocus setup to test the whole system, using the given panel. It is not the intent here to reproduce this extensive data but rather to show a few typical examples and to describe the test procedure.

3.4.1 Photo Response.

The setup used for measuring photo response is shown in Figure 2. A light source is projected by a lens and beam splitter onto the panel under test, and to a photomultiplier tube. For a given bias, e, on the panel, the photomultiplier current is measured by reading the voltage, V_1, across a load resistor. Similarly, the current through the panel is measured by reading the voltage, V, across load resistor R_L. Since the photomultiplier is linear with light input, V_1 will be proportional to the light flux falling on the panel and photomultiplier. By plotting V against V_1 as the light intensity is varied, we obtain the photo response. Figure 3 is a set of photo response curves for a typical binder panel. One electrical contact was the tin oxide layer and the other contact was pressure backed aluminum foil. In Figure 3 the y-axis is proportional to the signal current and the x-axis to the light input. Two points are worth noting: The photo response is non-linear (sub linear), and there is a difference in the photo response for forward bias as against reverse bias. This is to be expected, inasmuch as the aluminum to semiconductor contact forms a rectifying junction. In order to obtain ohmic contacts, metals such

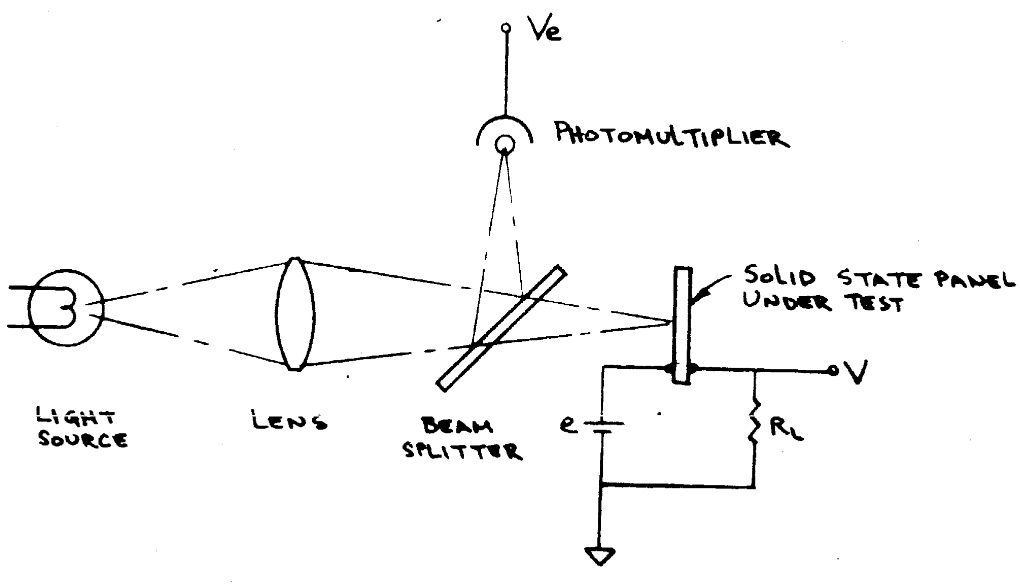

FIG 2 PHOTO RESPONSE MEASUREMENT SYSTEM

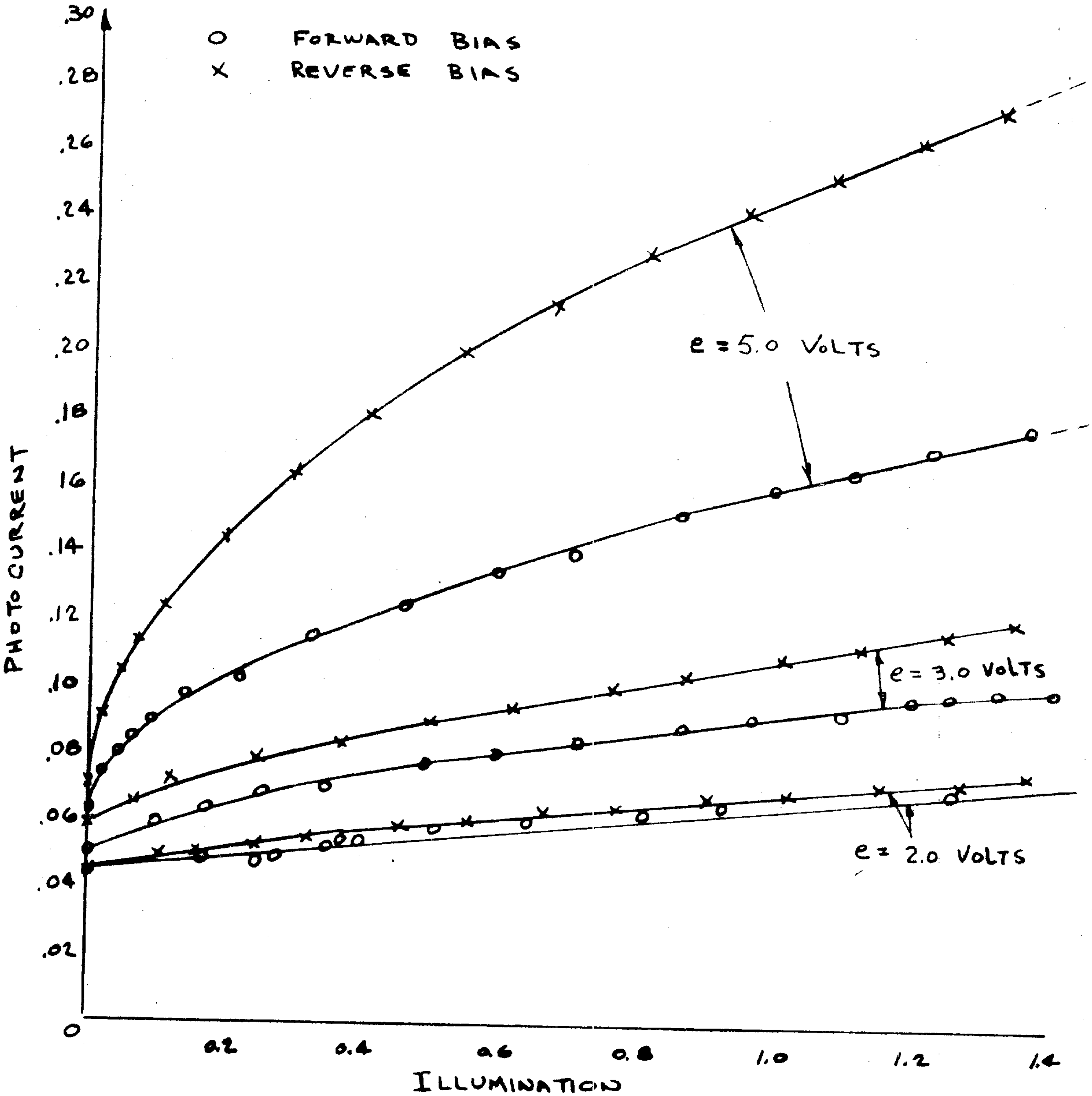

FIG 3 PHOTO RESPONSE OF BINDER PANEL

as gallium, indium or antimony would have to be used. For some applications the rectifying junction may be of advantage.

3.4.2 Current-Voltage Tests.

To plot the current-voltage characteristic of the panel, a setup is used which is similar to the one just described. The light intensity is kept constant and the bias voltage is varied. Figure 4 shows an i-v plot for a typical binder panel. This is repeated for several light intensities. For the curves in Figure 4, the light intensity was varied by insertion of neutral density filters in the light path.

3.4.3 Linearity Tests.

Either the photo response data described in section 3.4.1, and shown in Figure 3, or the i-v curves of Figure 4, can be used to obtain the degree of non-linearity. This is best done by plotting photo response on log-log paper and measuring the slope. Such a plot is shown in Figure 5. The data for these curves was obtained from the i-v characteristic of Figure 4. For this binder panel, the power law was approximately square root. The average slope was $m = 0.55$.

3.4.4 Uniformity Tests.

A test was made to check uniformity of response over the surface of the panel. For this test the panel was mounted in a microscope cross slide and a point source was imaged onto it. The panel was moved in x and y and the signal current monitored. Typical variations over the surface were about a factor of 4, even though some selected panels showed variations of less than 25% over a one square inch area. This non-uniformity could not be completely ascribed to the

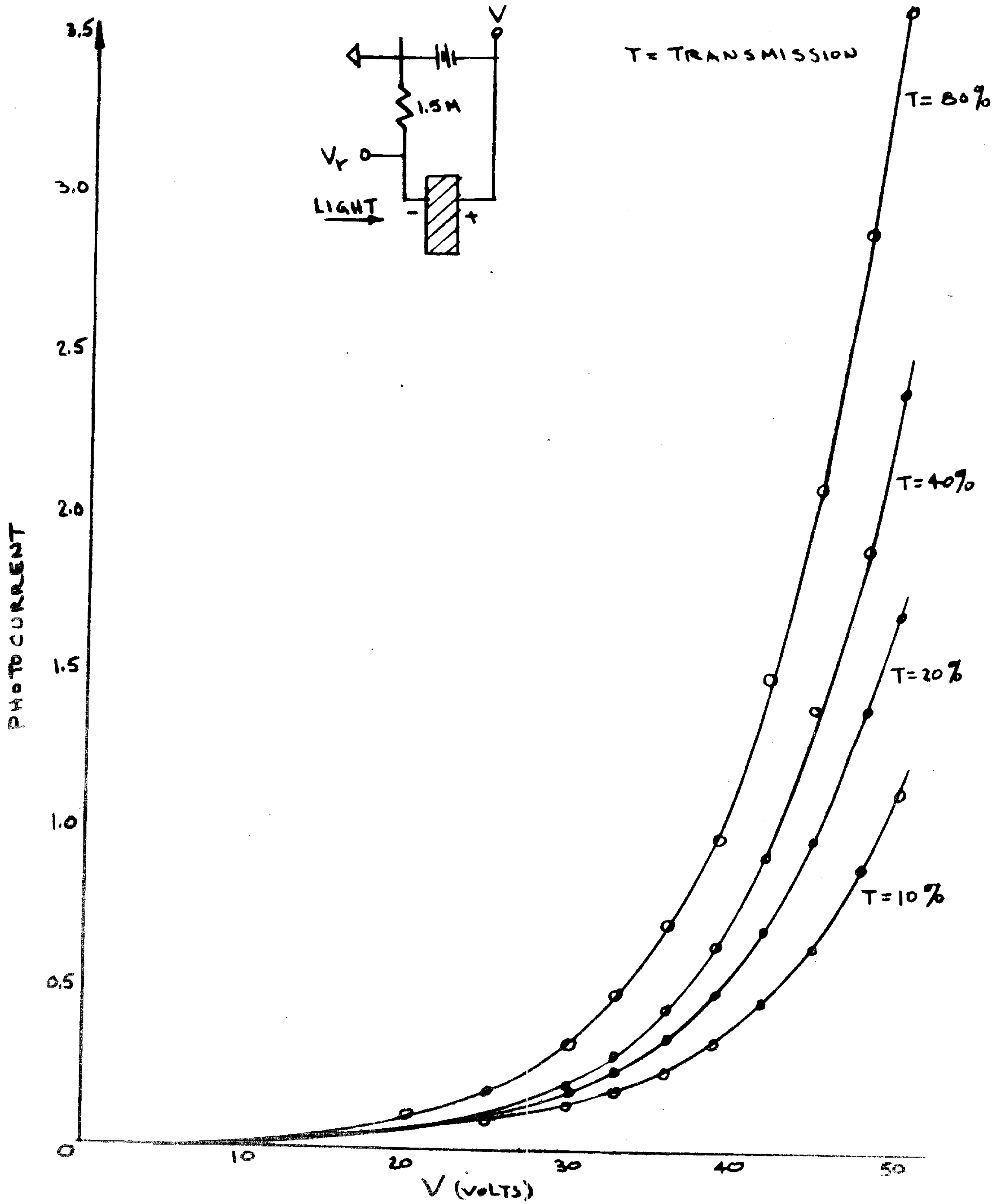

FIG 4 CURRENT - VOLTAGE CHARACTERISTIC

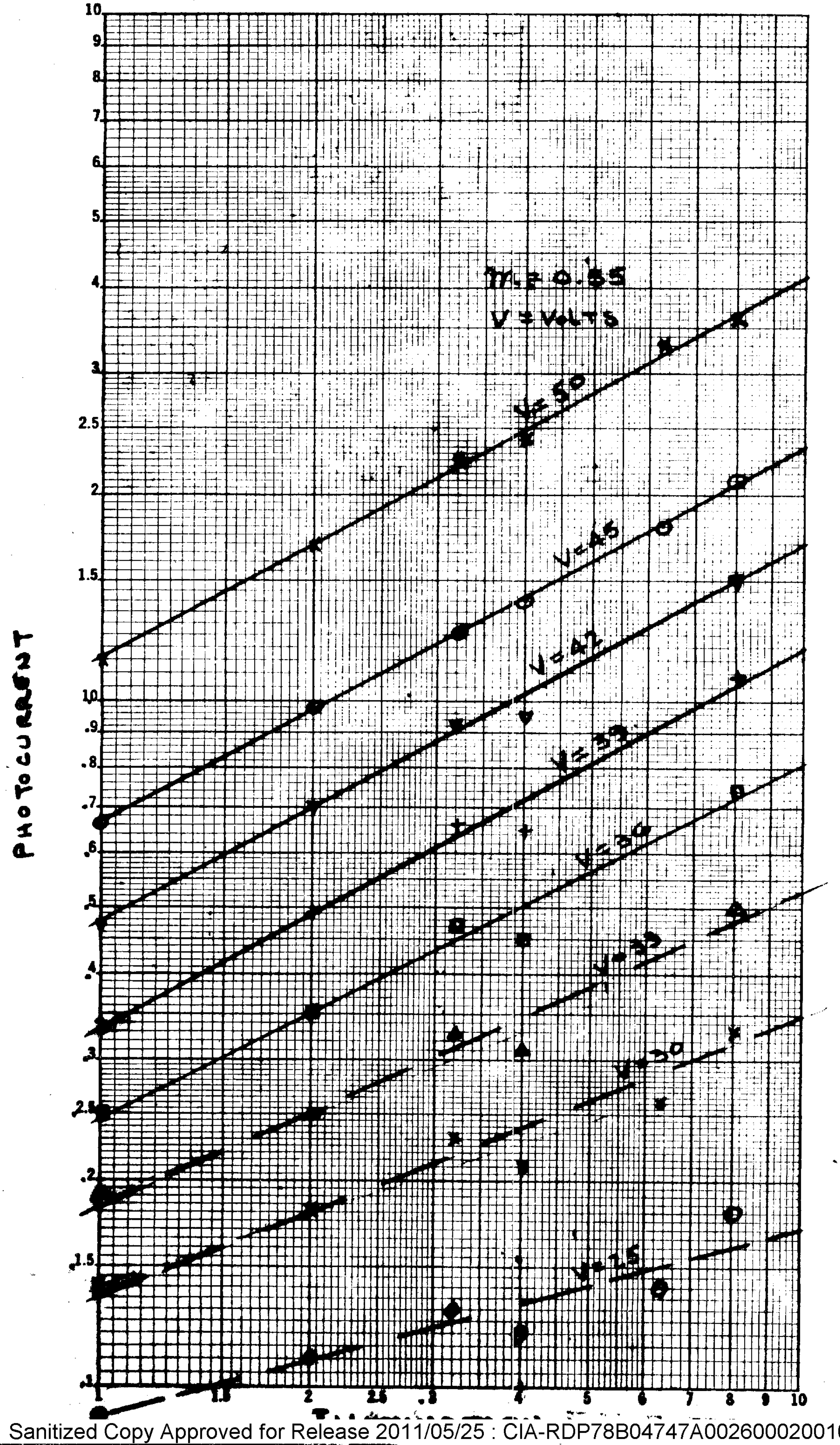

LINEARITY PLOT

FIG 5

25X1

photoconductor. With the pressure backed aluminum foil electrode, the electrical contact was not quite uniform, and this may contribute greatly to the observed variations in response. This is expected to improve dramatically by using evaporated indium contacts.

3.4.5 System Tests.

Suitable panels were selected by checking linearity, uniformity and sensitivity, as described above. These panels were then used in the autofocus test system to evaluate their performance. The test system is shown in Figure 6. A slide is illuminated by a tungsten source and condenser lens. The slide was mounted on a rack and pinion arrangement. It was focused by the objective lens and beam splitter onto the two panels. The output of the two panels (S_1 and S_2) could be monitored separately. These two outputs were also fed to a differential amplifier arrangement whose output S could also be recorded. The procedure was to move the slide through focus and record the three signals S, S_1, and S_2. The signals S_1 and S_2 show the response of the sensors to changes in focus, while S is a signal suitable for use in a feedback servo system to bring the slide back into focus automatically.

4.0 Results.

Using selected sintered panels, we were able to obtain good autofocus performance. Figure 7 shows the final results obtained. As such, they represent the major achievement and success scored in this development. Figure 7a shows the output signal from one panel, while the differential output, S, is shown in Figure 7b. As can be seen from the oscillograms, both the signal-to-noise ratio and sensitivity

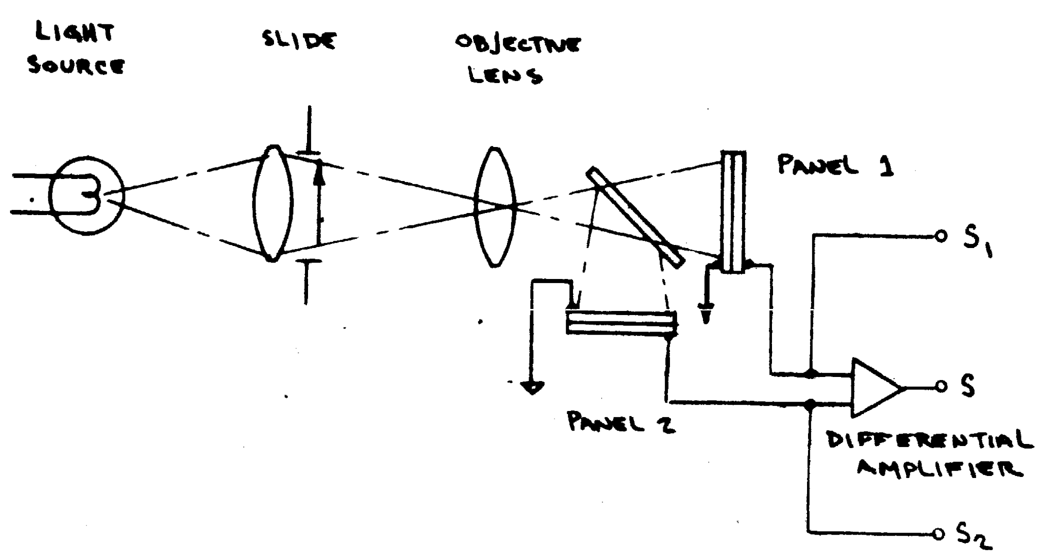

FIG 6 AUTO FOCUS TEST SYSTEM

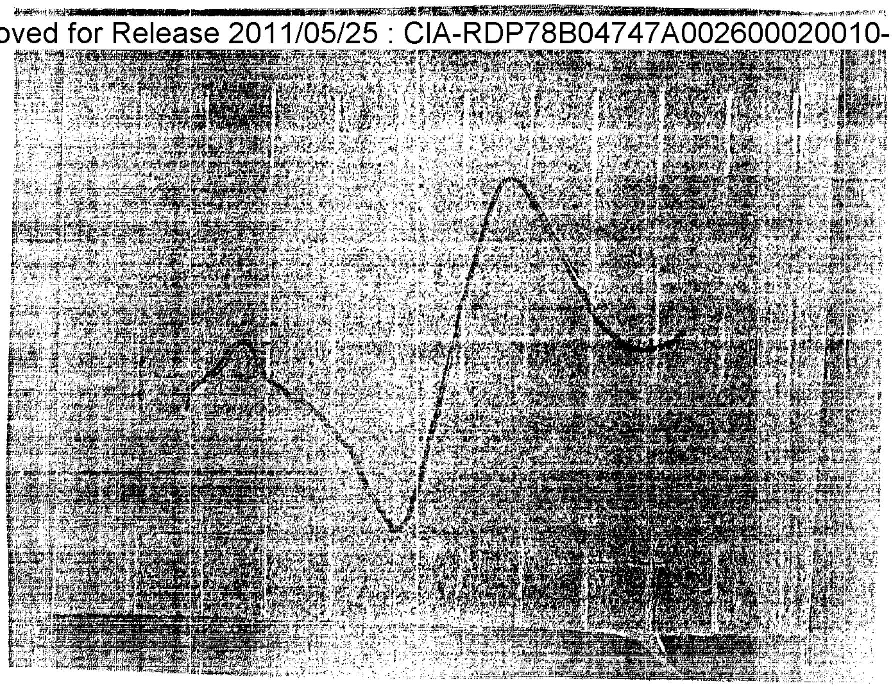

a) Differential Amplifier Output

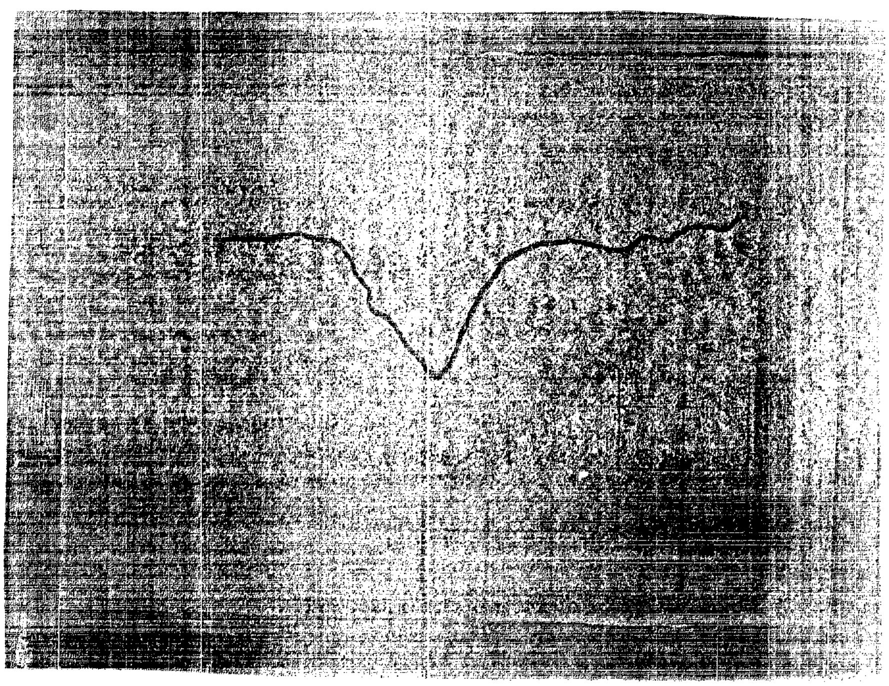

b) Output of One Panel

FIG. 7 AUTOFOCUS TEST RESULTS

25X1

to focus is adequate. The results of Figure 7 were obtained with the best pair of panels.

In Figure 7 the vertical sensitivity is 200 millivolts per cm. The horizontal sensitivity is 0.077 inches of object motion per cm. The measured noise was about 20 mV. The sensitivity of the discriminator signal, as can be seen on the oscillogram, was 4.25 volts per inch of object motion. The focusing accuracy should, therefore, be

$$\Delta X = \frac{\text{noise voltage}}{\text{sensitivity}} = \frac{0.020}{4.25} =$$

$$= 0.0047'' \cong 120\ \mu.$$

$120\mu\left(\frac{MM}{10^3\mu}\right) = .12MM = 8.35\frac{L}{MM} = \underline{4.16\frac{LP}{MM}}$

This performance was ≈10:1 obtained with continuous tone imagery of moderate contrast. Even better performance was gotten with a point source object.

5.0 More Recent Developments.

After the conclusion of work on this project, [redacted] has continued its development work towards attaining improved panel performance and more reproducibility between panels. The following techniques proved very successful: 25X1

1) Sequential sifting of powder to obtain smaller grain sizes.

2) Use of unfluxed powder and addition of the flux after deposition and before sintering.

3) Improved settling technique whereby the settling is done through a higher liquid column and performed in several stages.

4) Evaporated metal electrodes.

In addition to these, work is in progress on another method for preparing panels which holds great promise. This involves a technique for spraying the photoconductor onto a hot substrate and a subsequent firing at about 1200°F. This looks so promising that we delayed this report in the hope of being able to communicate first results obtained with this method. These, however, have been delayed and will be forthcoming in another three weeks.

5) Additional specialized test equipment was built which greatly facilitates the evaluation of panel performance.

6.0 Conclusions.

Using sublinear binder panels, it was possible to demonstrate the basic system principles. With the advent of the sintered panels enhanced performance was possible. The operation of an autofocus system was demonstrated and a signal suitable for driving a servo system was obtained. This, we feel, fulfills all the expectations that were anticipated at the outset of the project.

7.0 Recommendations.

In view of the fine results achieved thus far, it is felt that the work be continued with the aim of attaining an operational autofocus system to be incorporated into an

25X1

existing projector. This work, it is recommended, be divided into two phases: a sensor improvement phase and an engineering design phase.

Under the sensor improvement phase, the following performance objectives should be set:

1) Resolution of 20 lines per mm in the sensor plane.
2) Autofocus sensitivity of 30 microns.
3) Signal-to-noise ratio of 50 to 1.
4) Super-linear response with a square or higher power law.
5) Light to Dark impedance ratio of 500:1.
6) Rise time of 10 milliseconds.
7) Fall time of 5 milliseconds.
8) Uniformity of response of ± 5% over any 16 square millimeters, and ± 20% over 600 square mm.
9) Drift to be less than 15% per hour.

In order to achieve the above performance goals, the following techniques should be explored:

A. Sintering Technique.

1) Multiple layer sintering to eliminate pinholes.

2) Grazing angle contact evaporation onto the sintered layer to prevent low impedance paths.

3) Sintering in a nitrogen atmosphere at elevated pressures.

4) Spray application of flux material.

B. Spray Application Method.

1) Application of CdS and CdSe powders by spraying the powdered suspension onto the substrate.

2) Application of photoconductor by spraying liquid mixture of chemicals containing Cd and S ions, as for example CdCl and Thiourea.

C. Evaporation of CdS by a vapor phase reaction.

Under the engineering design phase the following objectives should be attainable:

1) Design amplifier, stabilizer, discriminator, and servo circuits to stabilize and compensate for any residual drifts until these are reduced to less than 2% between pairs of panels.

2) Design servo system to have a response of 10 cps.

3) Modify projector mechanically as needed to incorporate the autofocus system and provide for manual override.

25X1

[redacted]

Appendix A

For the solid state correlator the output signal is proportional to

$$\int \frac{f(x)\,f(x+\tau)}{f(x)+f(x+\tau)}\,dx,$$

where τ is the amount of misregistry. It would be of interest to evaluate this output signal for a typical image. Preferably, we should like to describe the typical image in such a way that the description may fit a wide range of imagery, at least in a statistical sense.

To do so, let us assume that the image is made up of rectangular objects of size n x m. Let us further assume that there are a whole range of such rectangles, each of different dimensions, and that each such rectangular spot has a gray shade u. Furthermore, we presume that the shade of gray is independent (statistically) of the size patch. The distribution of gray levels is given by p(u); i.e. the percentage of area having gray shades lying between u and $u+\Delta u$ is $p(u)\,\Delta u$. We also have to assume some distribution function for the patch sizes. A convenient distribution which is close to reality is,

$$p(n,m) = \frac{1}{\bar{n}^2\,\bar{m}^2}\, n\, m\, e^{-\frac{n}{\bar{n}}-\frac{m}{\bar{m}}}$$

where $\bar{n}$ is the average patch length in the x-direction and $\bar{m}$ in the y-direction. Actually, since the n and m are statistically independent we can work with one dimension, save ourselves some mathematical complexity, and then generalize to two dimensions. We thus take,

$$\rho(r) = \frac{1}{\bar{r}^2} e^{-\frac{r}{\bar{r}}} \quad ; \text{ FOR } r \geq 0 .$$

If we now have some function f(x) which consists of a series of these patches of varying gray shade and the same function shifted by an amount τ, then some patches having the same shade of gray will overlap. All those patches which are larger than τ will, in fact, overlap partially. Let us now calculate this percentage overlap, G.

The percentage of any one overlapping patch will be

$$g = \frac{r - |\tau|}{r} = 1 - \frac{|\tau|}{r}$$

The total amount of overlap will be the percentage overlap for each patch and summed over all patches larger than τ. Thus,

$$G = \int_{|\tau|}^{\infty} g\,\rho(r)\,dr = \int \left[1 - \frac{|\tau|}{r}\right] \frac{e^{-\frac{r}{\bar{r}}}}{\bar{r}^2}\,dr .$$

$$= e^{-\frac{|\tau|}{\bar{r}}}$$

25X1

We now have to evaluate the signal

$$Z = \int \frac{f(x)\, f(x+\tau)}{f(x) + f(x+\tau)}\, dx .$$

This may be written as,

$$Z = \overline{\left(\frac{v w}{v + w}\right)}$$

where the bar denotes the ensemble average and where we abbreviated,

$$v = f(x)$$
$$w = f(x+\tau)$$

For a statistical image of the sort being considered, the integration is, of course, an averaging operation.

There are two choices now: either v = w or v ≠ w. When a pulse overlaps (for n > τ) v = f(x) = w = f(x+τ). Otherwise, v and w are unrelated. Hence, in order to obtain Z we can treat the two cases separately. For v = w,

$$Z_0 = \overline{\left(\frac{v \cdot v}{v + v}\right)} = \frac{\overline{v}}{2} \quad ;$$

and for $v \neq 0$

$$Z_1 = \overline{\left(\frac{v w}{v + w}\right)}$$

Hence, $$Z = \frac{\overline{v}}{2} G + \overline{\left(\frac{v w}{v + w}\right)} [1 - G] ,$$

or $$Z = \frac{\overline{v}}{2} e^{-\frac{\tau}{n}} + \overline{\left(\frac{v w}{v + w}\right)} \left(1 - e^{-\frac{\tau}{n}}\right)$$

What is left to be done is to evaluate Z for the case when v and w are different and thus statistically independent. This is given by

$$Z_1 = \overline{\left(\frac{vw}{v+w}\right)} = \iint_{-\infty}^{\infty} \frac{vw}{v+w}\, p(v)\, p(w)\, dv\, dw.$$

For any arbitrary distribution of gray levels p(v), this is a most complex integration. For some simple cases, however, this can be worked out. Let us take a uniform distribution of gray shades,

$$p(v) = \frac{1}{c}$$

Then,

$$\bar{Z}_1 = \frac{1}{c^2} \int_0^c \int_0^c \frac{vw}{v+w}\, dv\, dw$$

This integral can be evaluated and shown to be,

$$\bar{Z}_1 = 0.2c$$

Hence, the complete expression now becomes,

$$\Xi = 0.25C\, e^{-\frac{|\tau|}{\bar{n}}} + 0.2C\left(1 - e^{-\frac{|\tau|}{\bar{n}}}\right)$$

$$= 0.05C\, e^{-\frac{|\tau|}{\bar{n}}} + 0.2C$$

For two dimensions, this becomes,

$$\Xi = 0.05C\, e^{-\left(\frac{|\tau_x|}{\bar{n}} + \frac{|\tau_y|}{\bar{m}}\right)} + 0.2C$$

In this manner we can predict what the correlator signal will be for an image whose average patch size is $\bar{n} \times \bar{m}$ and whose range of gray tones is from zero to C. This curve peaks at $\tau = 0$. The sharpness of the peak depends on $\bar{n}$ and $\bar{m}$, as well as on C.